

Fig. 7 Plate thickness vs fatigue life.

upon the examples discussed here, significant reductions in panel thickness (or weight) or increases in flight envelope may result from design on the basis of finite fatigue life. This emphasizes the need for an experimental investigation to assess the accuracy of available theory in predicting flutter stress levels and fatigue life.

#### References

- <sup>1</sup> Dowell, E. H., "Panel Flutter: A Review of the Aeroelastic Stability of Plates and Shells," *AIAA Journal*, Vol. 8, No. 3, March 1970, pp. 385-399.
- <sup>2</sup> Dowell, E. H., "Nonlinear Oscillations of a Fluttering Plate—II," *AIAA Journal*, Vol. 5, No. 10, Oct. 1967, pp. 1856-1862.

## Experimental Evaluation of a Subsonic Ludwig Tube

PHILIP C. MALTE\* AND KENNETH R. SIVIER†  
The University of Michigan, Ann Arbor Mich.

A SUBSONIC Ludwig<sup>1</sup> tube, or simple expansion tube, can supplement a shock tube as an aerodynamic testing facility. For example, the convective flow behind the centered expansion wave propagating in the tube can be used to accelerate small solid particles and thereby measure drag forces pertinent to two-phase flow systems. In the subsonic mode, the Ludwig tube has five times the useful flow duration of an equivalent length shock tube.<sup>2</sup> Furthermore, a Ludwig tube may complement a shock tube in studies concerning the effect of flow expansion on chemical reaction rates. However, before being used as an investigative device, the flow characteristics of the tube must be determined; the results presented herein summarize experiments conducted for this purpose and reported in Ref. 2.

The Ludwig tube tested consisted of a pipe 15 ft in length with a 3.1-in. i.d. The centered expansion wave was initiated at a diaphragm located between the pipe and a dump tank. Upon diaphragm rupture, the unsteady expansion wave, assumed centered at the rupture point, propagated upstream into the quiescent high-pressure air contained within the

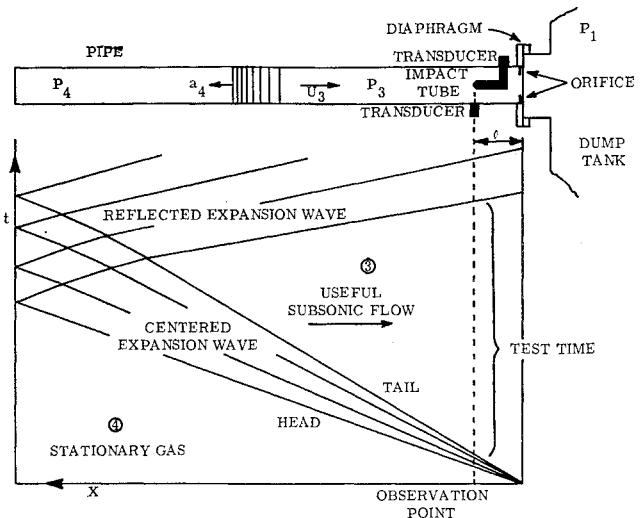


Fig. 1 Subsonic Ludwig tube.

pipe; the shock wave created at rupture spread into the dump tank and rapidly weakened. The shock wave was assumed of insignificant importance; the main change in the pressure level of the dump tank was caused by the mass addition. Furthermore, no reflected shock was ever observed in the pipe. The subsonic Ludwig tube with corresponding wave diagram is shown in Fig. 1. Pressure transducers and an impact tube were used to monitor static and total pressure 9 in. from the rupture point. Also, for comparison the static pressure was measured 3 ft from the rupture point. For flow Mach numbers below 0.7 the expansion wave was thin; the durations of the useful expanded flow were, respectively, 20 msec and 15 msec at the 9-in. and 3-ft observation points. The expansion wave approached "infinite" time duration for sonic conditions. All durations agreed closely with the isentropic unsteady theory of Ref. 3. Furthermore, the expansion wave as observed was always well formed, as indicated by typical pressure traces shown in Fig. 2.

The steadiness of the convective flow behind the expansion wave was examined in some detail. While several authors, principally Mirels,<sup>4,5</sup> have shown the effect of boundary layers on flow in shock tubes, we encountered few investigations concerning the flow behind an isolated unsteady expansion wave. In our investigation, the induced flow was quasi-steady, the second-order variations being caused by the action of the boundary layer and by the rising dump tank pressure. The effect of the boundary layer was further expansion; with increased distance behind the expansion wave (or increased time at a fixed observation point) the pressure decreased and the Mach number inferred from pressure measurements increased. The rising tank pressure induced weak compression waves that propagated upstream, thereby caus-

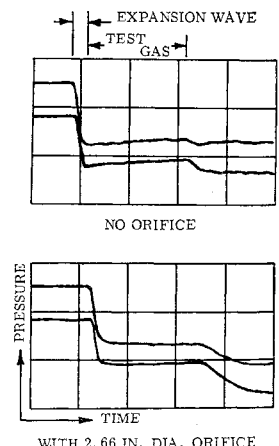


Fig. 2 Oscilloscope pressure traces: static pressure, top; impact pressure, bottom. 0.2 psi/div, 10 msec/div.  $l = 9$  in.,  $M_3 \approx 0.4$ ,  $Re \approx 1.8 \times 10^4$ .

Received April 20, 1970; revision received May 18, 1970. This work was supported by NASA Grant N1G 86-60.

\* Graduate Student, Department of Aerospace Engineering; currently on leave-of-absence from Martin Marietta Corp., Denver, Colo. Student Member AIAA.

† Associate Professor, Aeronautical and Astronautical Engineering Department, University of Illinois, Urbana, Ill. Member AIAA.

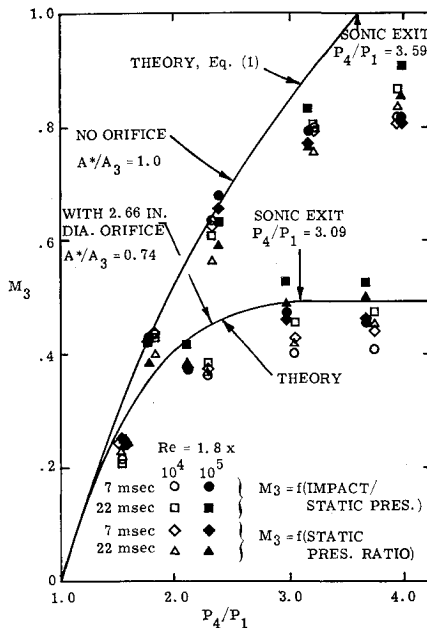


Fig. 3 Experimentally determined flow Mach number at 9-in. observation point.

ing an increase in pressure and decrease in the net convective velocity in the pipe. To reduce the effect of the compression system, orifice plates were mounted at the rupture point. With a choked orifice, the flow underwent "staged" unsteady and steady expansions to sonic conditions and further unsteady supersonic expansion.

Figure 3 shows the measured Mach number at  $l = 9$  in. for two test times—just after the expansion wave passed (7 msec) and just before the reflected expansion returned (22 msec)—with orifice-to-pipe area ratios of 0.74 and 1.0. Tests were conducted at two Reynolds numbers,  $Re$ , based on pipe diameter and the convective flow conditions, of about  $1.8 \times 10^4$  and  $1.8 \times 10^5$ . The Mach number was determined both by using the static pressure ratio across the expansion wave, i.e.,

$$M_3 = 2/(\gamma - 1)[(P_4/P_3)^{\frac{\gamma-1}{2\gamma}} - 1] \quad (1)$$

and by using the ratio of static to impact pressure measured in the convective flow. Theoretical predictions for air were obtained using Eq. (1) based on the initial diaphragm pressure ratio and the steady flow isentropic equations for the region of steady expansion immediately upstream of the orifice.

For the 2.66-in. orifice case of Fig. 3 at  $M_3 > 0.35$ , the exit was choked or nearly choked; also the expansion wave remained thin. Therefore, any change in the flow behind the expansion wave should have been due mainly to the unsteady boundary layer. As noted, the Mach number increased with time behind the expansion wave; there was a corresponding pressure decrease. Furthermore, the total pressure increased slightly, at  $\frac{1}{3}$  the rate for the static pressure change. Similar results were obtained for experiments at higher pressure levels wherein the Ludwig tube was discharged to ambient pressure. Thus, it appears that the boundary layer caused the convective flow to undergo a steady expansion similar to that encountered during subsonic flow through a converging channel. The results obtained with no orifice show the spreading of the expansion wave near sonic conditions; unity Mach number never was attained. At flow Mach numbers near 0.6, the Mach number decreased with time, indicating increased pressure due to the tank induced compression system.

The consistent differences between the two methods of Mach number determination indicated in Fig. 3 can be ex-

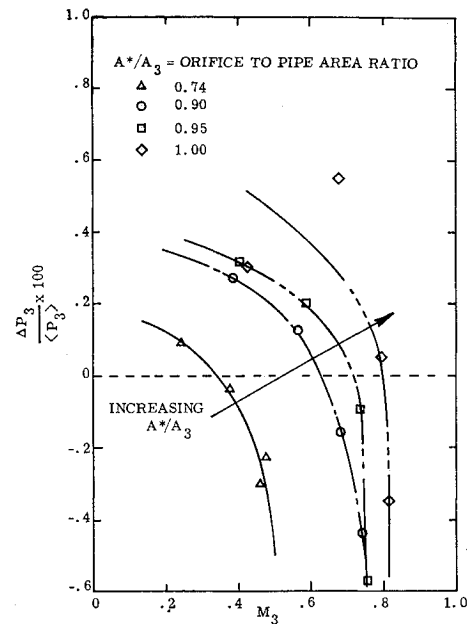


Fig. 4 Percentage change in pressure in flow behind expansion wave at  $l = 9$  in.,  $Re \approx 1.8 \times 10^4$ .

plained since the right running Riemann variable  $[2a/(\gamma - 1) + U]$ , upon which Eq. (1) is based, was no longer constant in the slightly two-dimensional flow behind the expansion wave. Thus Eq. (1) does not describe sufficiently the flow with a finite boundary layer. Also, a slight Reynolds number dependence is noted in Fig. 3; the higher Mach numbers measured at the higher value of  $Re$  indicate a greater flow constriction by the boundary layer which became turbulent during the flow period for the  $Re = 1.8 \times 10^5$  case.

With an orifice of proper size, it was possible, in effect, to cancel the opposite contributions of boundary-layer growth and rising tank pressure. As shown in Fig. 4, a constant pressure flow is obtained by increasing the orifice size for increased Mach number. The influence of the orifice in reducing compressions and yielding flow steadiness is noted by comparing the two traces of Fig. 2 for similar flow Mach numbers with and without an orifice.

The boundary-layer thickness and character were found to be dependent on the Reynolds number,  $Re_x$  based on the distance that an accelerated fluid element had traveled. It was assumed that the gas was accelerated instantaneously from zero velocity to the convective flow velocity at the expansion wave center; this appears valid for thin expansion waves corresponding to flow Mach numbers below 0.7. By immersing the impact probe in the boundary layer, transition was found to occur at  $Re_x = 1.9 \times 10^6$ . Varying the radial location of the impact probe indicated that the constant velocity central core of the flow had a radius greater than  $\frac{1}{2}$  the pipe radius for  $Re = 1.8 \times 10^4$ . However, at  $Re = 1.8 \times 10^5$  transition occurred during the period of convective flow, and consequently the central core was reduced. Velocity profiles obtained at  $Re_x = 5.7 \times 10^6$  (corresponding to  $Re = 2 \times 10^6$  at 22 msec) indicated that the flow was rapidly approaching fully developed turbulent pipe flow.

This study has shown that the subsonic Ludwig tube can provide a quasi-steady flow of sufficient steadiness and length to be useful as an aerodynamic testing device. It appears that appreciably longer flow times and larger Reynolds numbers can be obtained by using longer and larger diameter tubes.

## References

- 1 Ludwig, H., "The Pipe Wind Tunnel," Dec. 1956, Langley Aeronautical Laboratory, NACA; Translation of "Der Rohr-

windkanal," *Zeitschrift für Flugwissenschaften*, Vol. 3, No. 7, 1955.

<sup>2</sup> Malte, P. C. and Sivier, K. R., "Experimental Evaluation of a Subsonic Expansion Tube," CR-1354, June 1969, NASA.

<sup>3</sup> Courant, R. and Friedrichs, K. O., *Supersonic Flow and Shock Waves*, Interscience, New York, 1948.

<sup>4</sup> Mirels, H., "Boundary Layer Behind Shock or Thin Expansion Wave Moving into Stationary Fluids," TN-3712, May, 1956, NACA.

<sup>5</sup> Mirels, H., "Test Time in Low-Pressure Shock Tubes," *The Physics of Fluids*, Vol. 6, No. 9, September, 1963, pp. 1201-1214.

## Velocity Profile Measurements in a Spinning, Cold-Flow Rocket Motor

GEAROLD R. JOHNSON\* AND MEL R. L'ECUYER†  
Purdue University, Lafayette, Ind.

### I. Introduction

A PROBLEM of considerable experimental and theoretical interest is the description of the interior ballistics of a spinning, solid-propellant rocket motor. This interest has developed since the use of spin stabilized, solid-propellant rocket motors has shown that the actual performance under spinning conditions differed substantially from the performance predicted from nonspinning, solid-propellant rocket motor data.

The purpose of the investigation reported herein was to study the effects of rotation on the flow field inside the chamber of a simulated end-burning rocket motor. In particular, the cold-flow study offered the possibility of the use of a velocity probe for determining the profiles of the axial and tangential velocity components within the chamber of the spinning, cold-flow rocket motor.

### II. Apparatus

The apparatus used for this investigation was used in the vortex choking studies conducted by Norton, Farquhar, and Hoffman.<sup>1</sup> Basically, the apparatus consisted of a stationary air-feed chamber and a rotating rocket motor chamber and nozzle. The rocket motor chamber was connected to the air-feed chamber by means of a hollow drive shaft. The

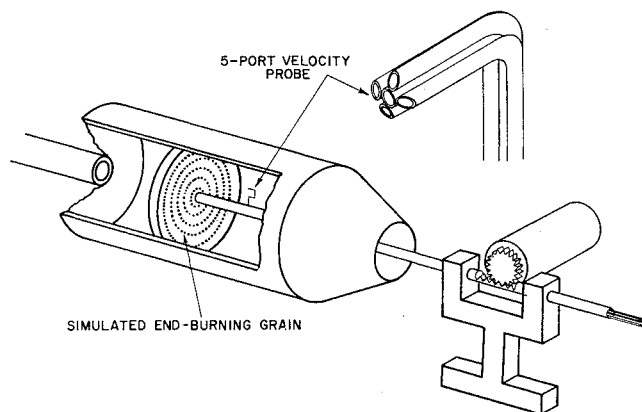


Fig. 1 Cold-flow rocket motor and velocity probe arrangement.

Received April 27, 1970. This research was supported by the Propulsion Laboratory, U.S. Army Missile Command, Redstone Arsenal, Ala., under Contract DA-01-021-AMC-15257(Z).

\* Research Assistant in Mechanical Engineering.

† Associate Professor of Mechanical Engineering. Member AIAA.

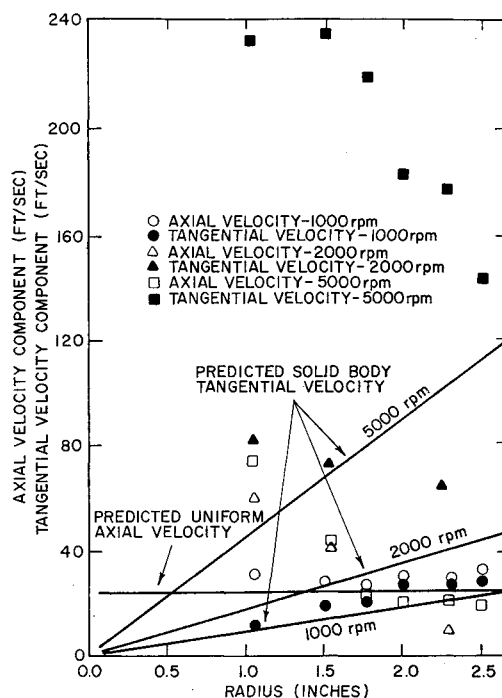


Fig. 2 Velocity profiles — 1.125 in. nozzle.

rocket motor was supported horizontally and was rotated about its longitudinal axis by an air turbine directly connected to the hollow drive shaft. Air was supplied to the head end of the rocket motor chamber via flow from a set of storage tanks, through a metering orifice and the hollow drive shaft. The air passed through a porous surface to simulate the flow emanating from an end-burning grain. The simulated end-burning grain consisted of a sintered steel plate which was used to produce a large axial pressure drop to minimize the variation of the local mass flow per unit area across the grain surface due to the increasing radial pressure gradient with rotation.

Figure 1 illustrates schematically the general arrangement of the cold-flow rocket motor and the mechanism employed

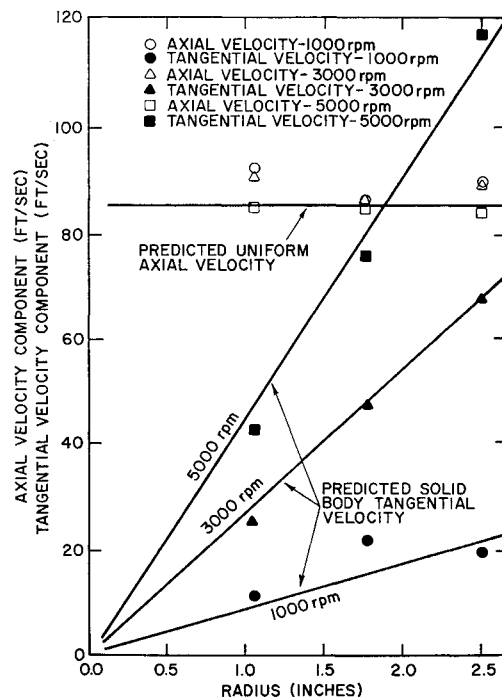


Fig. 3 Velocity profiles — 2.0 in. nozzle.